The importance of subsurface lithology in controlling magma storage versus eruption: an example from offshore southern Australia

P. Reynolds[1], S. Holford[1*], N. Schofield[2], A. Ross[3]

[1] Centre for Tectonics, Resources and Exploration (TRaX), Australian School of Petroleum, University of Adelaide, Adelaide, SA 5005, Australia

[2]Department of Geology & Petroleum Geology, University of Aberdeen, Aberdeen AB24 3UE, UK

[3]CSIRO Energy, Australian Resources Research Centre, 26 Dick Perry Avenue, Kensington, WA 6151, Australia

*Corresponding author: simon.holford@adelaide.edu.au +61483138035

Abstract

The volumetric relationship between the intrusive and extrusive components of volcanic fields are difficult to constrain. This is because the erupted products are commonly either eroded, or the intrusions are concealed by overburden. 3D seismic data therefore offers a unique opportunity to study ancient volcanic provinces, since these datasets can image both components without the need for erosional dissection. This study is based on 3D seismic data from the Bight Basin Igneous Complex (BBIC); a volcanic province constructed within a sedimentary basin, offshore southern Australia. We demonstrate that the BBIC contains abundant sills and laccoliths emplaced within deltaic sediments. The intrusions have a total volume of 92–111 km^3 whilst the lava flows and volcanoes have a combined volume of 66–76 km^3 (Dense Rock Equivalent). This indicates that the ratio of intrusive:extrusive

products for the BBIC is between 1:1 and 2:1. The architecture of the BBIC contrasts markedly with the neighbouring Newer Volcanics Province (NVP), which lacks abundant sills and laccoliths. Since lava flows and volcanoes in the NVP were dominantly fed by dykes hosted in basement rock, we suggest subsurface lithology plays an important role in causing sill formation and determining the total volume of magma stored in the subsurface.

Introduction

A fundamental goal of volcanology is to understand the relationship between the magma stored in the subsurface and that erupted at the surface. Quantification of the relative proportion of these components (the intrusive:extrusive or "I:E" ratio) can be used to predict the magnitude of future eruptions (Ferguson et al., 2010), to determine the volumes of magma intruded beneath active volcanic provinces, and provide insights into volcanic processes on other planets (Greeley and Schneid, 1991). The intrusive component is commonly represented by igneous bodies such as sills, laccoliths and dykes (e.g. Jackson et al., 2013; Schofield et al., 2015). Subsurface stalling of magma, to form intrusions, can be caused by insufficient magma driving pressure (Lister and Kerr, 1991), too high a magma density (Ryan, 1987), strong subsurface lithological control (Schofield et al. 2012), thermal death because of cooling (Taisne and Tait, 2011), viscous death due to decompression-induced crystallisation (Annen et al., 2006) or stresses created by overlying volcanoes (Pinel and Jaupart, 2004). In contrast, eruptions at the Earths' surface are ultimately driven by magma buoyancy and are manifested as lava flows and pyroclastic constructs. In intraplate volcanic fields (i.e. those unrelated to plate boundary processes; Schmincke, 2004) the total volume of magma erupted can provide insights into the mechanisms driving volcanism (e.g. Valentine and Perry, 2007).

Previous work has reported a wide range of I:E values, ranging from 1:1 to 16:1 (Shaw, 1980; Wadge, 1980; Crisp, 1984) and an "average" value of 5:1 (White et al., 2006).

Although ratios higher than 10:1 are uncommon (White et al., 2006), values of up to 180:1 have been reported from the Afar rift (Ferguson et al., 2010). The I:E ratio is thought to be related to factors including: 1) local crustal thickness; 2) tectonic setting; 3) the orientation and magnitude of principal stresses; 4) magma composition; and 5) the melt generation rate in the source region (White et al., 2006). There is not thought to be any systematic variation in I:E ratio with eruptive style, volcanic setting or total volume, although higher I:E ratios have been hypothesied to occur in regions of thicker crust (White et al., 2006). This is the result of the increased transit time for magma, which increases the potential for magma cooling (Shaw, 1980).

One approach to determine the I:E ratio is to make measurements of the magma plumbing systems beneath active or dormant volcanoes. For instance, mapping of incompatible elements, gravity surveys, flexural models and sulfur output by magma degassing can all be used to estimate the volume of the magma chamber (Allard, 1997; Haederle and Atherton, 2002; Vidal and Bonneville, 2004). Seismic, geodetic and electromagnetic methodologies can also reveal the dimensions of (partially) molten magma chambers (Iyer, 1984; Patanè et al., 2017). However, these methods are limited by their ability to directly observe the magma reservoir(s), and by the fact that the size of the magma bodies does not necessarily represent the total intrusive history, which is more long lived than individual magma reservoirs (White et al., 2006). Other studies have used measurements of overburden deformation to determine the geometry and emplacement depth of magma reservoirs (e.g. Lu et al., 2010). However, recent work has shown that the magnitude of ground deformation can be less than half the volume of the associated intrusion (Jackson et al., 2013) and that magma can be intruded without associated folding (Schofield et al., 2012). Alternatively, it is possible to measure the volume of ancient magma plumbing systems, and estimate the volume of the now-eroded erupted products (e.g.

Richardson et al., 2015). This method is inherently limited by its inability to directly observe the extrusive features.

3D seismic data offers a unique opportunity to investigate the I:E ratios of volcanic systems. Volcanic rocks buried within sedimentary basins are typically imaged at a high resolution, especially if they are buried at shallow depths (e.g. Reynolds et al., 2017a). These datasets allows insights into the relationship between the intrusive and extrusive components, without the need for erosional dissection. However, whilst previous work from magmatic-affected sedimentary basins has documented the distribution of intrusions and the architecture of lava flows and volcanoes (Thomson, 2005; Reynolds et al., 2017a), few studies have explicitly documented the volumetric relationship between these components. This is largely the result of sparse data coverage not permitting the I:E ratios to be accurately constrained (e.g. Magee et al., 2013), or the intrusive and extrusive products being spatially unrelated (Schofield et al., 2015; Reynolds et al., 2017b).

In this study we use newly acquired 3D seismic data from the Bight Basin Igneous Complex (BBIC), an intraplate basaltic volcanic field, located offshore southern Australia, which developed during a constrained time period during the early Middle Eocene (Schofield & Totterdell, 2008). This extinct igneous complex contains lava flow fields, volcanoes and a variety of sills and laccoliths. The extrusive features have their basal contacts at the same stratigraphic surface, which is also variably folded by underlying intrusions, indicating that intrusive and extrusive magmatism occurred concurrently (Schofield & Totterdell, 2008; Magee et al., 2013; Reynolds et al., 2017c). The near pristine preservation of volcanoes and lava flow fields within the province implies that it has largely been unaffected by erosion (Reynolds et al., 2017d), and the measured intrusive and extrusive volumes are likely to be representative of the entire lifetime of the volcanic field. We demonstrate that the volume of the sills and laccoliths is equal to as much as twice the volume of the volcanoes and lava

flows. We first describe the character of the components of the BBIC in seismic section, before calculating the volume of the extrusive and intrusive products and comparing this volume, and their ratio, to that of other volcanic provinces.

Geological setting

The Ceduna sub-basin is a NW-trending depocentre within the Bight Basin which is located on the rifted southern continental margin of Australia (Fig. 1). It contains a 15 km-thick sequence of predominantly sedimentary rocks. The sedimentary rocks were mostly deposited from the mid- to late-Jurassic to latest Cretaceous in response to continental rifting which culminated in break-up around 85 Ma, with a thin Cenozoic post-rift succession (Norvick, 2005). The sub-basin also hosts a series of mid-Eocene aged intrusions, volcanoes and lava flows within a 50,000 km^2 area known as the Bight Basin Igneous Complex (Schofield and Totterdell, 2008). The BBIC is one of several volcanic provinces along the southern Australian margin, which although classified as magma-poor, has undergone several post-rift phases of magmatism from the Eocene until the Holocene. The genesis of magmatism along the margin is not completely understood, but has been proposed to arise from factors such as impingement of hotspots beneath the crust; transtensional decompression of the crust and edge- and shear-driven convection of the mantle (Demidjuk et al., 2007; Conrad et al., 2011; Davies et al., 2015; Cas et al., 2016). Provinces found elsewhere along the margin include the 10−4.6 Ma Macedon-Trentham Province, Victoria; the 95−19 Ma aged Older Volcanic Province, located in Eastern Victoria; and the most widely studied 4.5 Ma – 4.5 kyr Newer Volcanics Province, located in Victoria and South Australia (Fig. 2; Wellman and McDougall, 1974; Edwards et al., 2004; Cas et al., 2016). Additionally, Cenozoic lava flows, volcanoes and intrusions are also found offshore in the Bass Basin and onshore Tasmania (Johnson et al., 1989; Reynolds et al., 2017a).

Intrusions within the BBIC were emplaced into the Paleocene−Eocene-aged Wobbegong Supersequence, the Upper Cretaceous-aged Hammerhead Supersequence and Middle Cretaceous-aged Tiger Supersequence, at depths of ~100 to 1200 m below the paleoseabed, with the shallowest intrusions generally found basinward (Reynolds et al., 2017c). The lava flows and volcanoes downlap the top of the Wobbegong Supersequence (Fig. 1). Cold-water, giant bryozoan reef mounds penetrated by the Potoroo-1 well are also found downlapping the base of the top of the Wobbegong Supersequence (Langhi et al., 2016) suggesting that the volcanoes and lava flows were emplaced in a submarine environment (Schofield and Totterdell, 2008; Jackson, 2012; Magee et al., 2013; Reynolds et al., 2017d). Dredging from incised canyons collected detrital volcanic fragments that were characterised as amygdaloidal, possibly pillowed, alkali basalts (Clarke and Alley, 1993) suggesting that the volcanoes have a similar composition (Schofield and Totterdell, 2008; Magee et al., 2013).

Dataset and Methods

Seismic reflection data

This study uses zero phase, time migrated, 3D seismic reflection data (the Nerites 3D survey) that was collected in 2014 by TGS, and covers an area of 9,000 km^{2-}(Fig. 1). The survey has a bin spacing and thus horizontal resolution of 12.5 × 15 m. The resolution ($\lambda/4$ where λ is seismic wavelength) and detection limits ($\lambda/30$) for intrusions are calculated to be >5 and >45 m, and for volcanic features these are calculated to be >4 and >40 m respectively, as explained in more detail subsequently. Our dataset covers the largest concentration of igneous features within the BBIC, with some volcanic features falling outside the Nerites survey. A trough event (i.e. a downwards increase in acoustic impedance, such as the transition from a sedimentary rock into a high density volcanic rock) is represented by a blue reflection. A peak event (i.e. a downwards decrease in acoustic

impedance, such as the transition from a high density volcanic rock into a sedimentary rock) is represented by a blue reflection.

Seismic interpretation strategy

Key seismic horizons interpreted within the survey include: 1) the Base Dugong; 2) the Top Vent; 3) the Top Extrusives; 4) the Top Intrusion; and 5) the Base Intrusion. The Base Dugong horizon was mapped across the entire survey. This horizon is a moderate-high amplitude, trough event which is folded above many intrusions (Schofield and Totterdell, 2008; Jackson et al., 2013). The Base Dugong is also onlapped by overlying sediments and downlapped by the volcanogenic vents and lava flow fields. Previous work using regional 2D seismic data strongly implies that the Base Dugong represents the paleo-surface at the time of magma intrusion and extrusive activity (Schofield and Totterdell, 2008; Jackson et al., 2013; Reynolds et al., 2017d).

The volcanoes are all found at the same stratigraphic interval (Schofield and Totterdell, 2008; Reynolds et al., 2017d). These volcanoes vary from 60 to 625 m in height and 0.3 to 10 km in diameter (see Reynolds et al., 2017d). The tops of the volcanoes are identified as the Top Vent and their bases are represented by the Base Dugong horizon. We therefore mapped one Top Vent reflection across each of the volcanoes in the survey. The reflection varies from low to high amplitude and from trough to peak events. The reflection may vary in character from smooth to rough and continuous to semi-continuous. The Top Vent reflection is onlapped by the overlying Dugong Supersequence which may be domed above the centre of the volcano (Fig. 3).

As with the volcanoes, all the lava flow fields are also located at the same stratigraphic interval, directly above the Base Dugong horizon. This enables mapping of the lava flow fields with one horizon, named the Top Extrusive. This horizon corresponds to the top of the lava flow fields and is high amplitude, sub-horizontal and terminates abruptly. It forms a

trough-peak couplet, beneath which the quality of seismic imaging is commonly reduced (Fig. 3).

The seismic interpretation method for intrusions differs from that of conventional time-surface mapping (Planke et al., 2005). For instance, intrusions can transgress the stratigraphy and may overlap with each other. Therefore, we mapped each intrusion with an individual Top Intrusion horizon. These horizons are mapped on high amplitude, trough events (Fig. 3). Once interpreted, they allowed us to produce depth-converted grids for the top of each intrusion. Similarly, we mapped an individual Base Intrusion horizon for each igneous body. These horizons are mapped on low-moderate amplitude, peak events. Beneath these horizons, the quality of seismic imaging is reduced, typical of volcanic rocks in seismic data which reflect and attenuate seismic energy (e.g. Jerram, 2002). In regions where the events marking the Base Intrusion horizons were not visible (i.e. the thickness of the intrusion was below the resolution limit of the data; see following text) the intrusions were represented by a single trough-peak doublet. In this case, we picked the peak event of the doublet as the Base Intrusion. This method allowed us to produce depth-converted grids for the approximate base of the intrusions. The inability to clearly identify the bases of some intrusions introduces some uncertianity into the calculation of their volumes. An additional source of uncertainity occurs in regions where intrusions vertically overlap, as the deeper intrusions are likely to be less clearly resolved, indicating that their volume estimates should be regarded as minima.

Method and Accuracy of Volume Calculations

There are no wells penetrating the igneous features in the Ceduna sub-basin. Measurements of intrusion thickness are therefore depth-converted assuming a velocity of 5500 m s^{-1}, which is representative for many intrusions that have been penetrated by drilling (Skogly, 1998; Smallwood and Maresh, 2002; Hansen and Cartwright, 2006). The dominant

frequency of the seismic data at the depth at which the intrusions are found is 30 Hz, indicating that the resolution limit of the data (i.e. the minimum thickness at which both the top surface and the bottom surface of the intrusions can be identified as separate reflections) is around 45 m, whilst the detection limit (i.e. the minimum thickness at which the intrusion is visible in seismic data) is around 5 m. Therefore, for a given intrusion where the top and bottom surface of the intrusion cannot be resolved and is 'tuned', the intrusion can range in thickness from 45 m to 5 m. Based on the potential variation in their velocity (e.g. Nelson et al., 2009), these values likely represent the minimum thicknesses that can be detected and resolved.

For each mappable intrusion, we calculated a minimum and maximum volume (e.g. Fig. 4). The maximum volumes were calculated by totalling the volume of the intrusion >45 m thick with the volume of the intrusion equal to or lower than the resolution limit (45 m), and assuming that the intrusions have a minimum thicknesses of 45 m. The minimum volumes of the intrusions were calculated in a similar method, only in this case assuming that the intrusions have a minimum thicknesses of 5 m in regions where their thickness is equal to or below the resolution limit. Varying the assumed velocity of the intrusions by 10% results in a corresponding change in the estimated minimum and maximum volumes (similar changes apply to ±10% variations in the assumed velocity of mapped volcanic features). The total volume of magma intruded into the basin was calculated by summing the volume of all the individual intrusions. We note that no dykes are directly observed in the seismic data, and thus it is not possible to estimate their volumes. The probable role of dykes in transporting magma in the BBIC is detailed in the Discussion.

The volume of the lavas was calculated assuming that the thickness of the lavas is between the detection limit and resolution limit of the data (i.e. they are represented by only a single trough-peak couplet). Based on the dominant frequency of the seismic data at

the depth at which the lavas are found (25 Hz) and using a velocity of 4000 m s^{-1} (Nelson et al., 2009) we calculate that the detection and resolution limits for the lava flow fields are 4 and 40 m respectively. Similar to the method employed for the intrusions, we therefore calculated a minimum and maximum volume of the lava flows using each of these thicknesses. We then converted the volumes of the lava flow fields measured in seismic data to their dense rock equivalent (DRE). Since the BBIC was constructed in a submarine environment (see 'Geological setting'; also Schofield and Totterdell, 2008; Jackson, 2012; Magee et al., 2013) we assume that all the lava flows have a vesicularity of 20%, comparable to that of pillow lavas (Jones, 1969). We use this value to calculate that the volume of individual lava flow fields.

The volumes of the volcanoes were calculated by first determining their internal velocity. We follow the approach of Magee et al. (2013) whereby their internal velocity was calculated from the thickness of pull-ups beneath the volcanoes or using a velocity of 2215 m s^{-1} (equal to the overlying Dugong Supersequence; as constrained by the Gnarlyknots-1 well) in cases where pull-ups were absent. We therefore suggest that each volcano has a velocity of between 2215−4900 m s^{-1}. These values were used to calculate volcano height. The volumes of the volcanoes were then converted to DRE assuming a vesicularity of 20%, as for the lava flows, with a ±10% variation in assumed vesicularity resulting in a concomitant change in estimated volume. The velocity of the Dugong Supersequence and frequency of the seismic data suggest that the data has a resolution limit of 30 m within these sediments.

Interpretation of the Bight Basin Igneous Complex

Volume of the intrusive and extrusive components

Seismic mapping has identified a total of 39 sills and laccoliths, 89 cone-shaped volcanoes and 26 lava flow fields (Fig. 5). The dimensions of these features are summarised

in Table 1. We also calculated the area covered by these features (Table 1) to compare them with the proportion of volcanic features outside the Nerites survey (see section on 'Seismic data' following text). Our data indicates that the combined volume of the intrusions imaged within the Nerites 3D seismic survey ranges from 92−111 km^3 (Fig. 6). The erupted products cover an area of 1160 km^2 and our estimate of their total DRE is 66–76 km^3. Our data therefore indicates an I:E ratio of between 1:1 and 2:1, with the volume of the intrusive component outweighing the volume of the lava flows and volcanoes. As evidenced by Fig. 7, the BBIC has an I:E ratio typical of continental volcanic provinces although the volume of the extrusive components is fairly low for basaltic volcanic fields (Fig. 8).

The role of dykes in vertical magma transport

Approximately 60% of the volcanoes and lava flow fields are linked to the shallowest tips of the proximal underlying intrusions (Reynolds et al., 2017c). Therefore, we infer that dykes acted as feeders for 40% of the volcanoes and lava flows within the Nerites survey (i.e. the extrusive features not underlain by sills or laccoliths). Based on the isolated distribution of the sills and laccoliths, the dykes are also interpreted to have played an important in feeding the concordant intrusions (Reynolds et al., 2017c). Many of these dykes are inferred to have propagated up faults, since the source regions of the sills and laccoliths are found above them (Reynolds et al., 2017c). The lengths of the dykes is unknown; dykes do not propagate to equal heights along their length (e.g. Keating et al., 2008).

Rates of magma production

The Nerites 3D seismic dataset can be used to estimate the duration and rate of magma eruption in the BBIC. All magmatism occurred during the mid-Eocene, evidenced by the superposition of all extrusive components directly onto the BD horizon and the forced folding of the BD caused by the underlying intrusions. Assuming a sedimentation rate of 15 m in 1 million years during the Eocene (based on nannofossil data collected during IODP Leg

182 to the west of our study area; see Li et al., 2003), and that the seismic data has a resolution of 30 m within the Dugong Supersequence (see section on 'Seismic interpretation strategy'), we estimate that no more than 2 million years could have elapsed before the entire BBIC was constructed. If the BBIC had been constructed over longer timescales, the extrusive features would not directly overly the BD due to inter-eruption sedimentation and the tops of the forced folds would not consistently be represented by the BD horizon. Therefore, based on seismic mapping, we calculate 72 km^3 of magma was erupted within a 2 Myr period. As a minimum estimate, this implies an eruption rate of ~36 km^3/Myr or 3.6×10^{-5} km^3/yr in the BBIC. If we assume that the BBIC was constructed over a shorter timescale, this would require an increased eruption rate (i.e. 144 km^3/Myr if constructed within 0.5 Myr).

Discussion

How much of the intrusive complex are we missing?

Our measurements indicate that the volume of the intrusions component outweighs that of the extrusive component by as much as 2:1. There are several reasons for which we consider our estimates of the intrusive components of the BBIC to be a minimum estimate. Firstly, well data from the Atlantic Margin, UK, suggests 63% of the intrusions within the subsurface are ≤5 m thick (Schofield et al., 2015). Assuming that other basins have similar distributions of sill thicknesses (as evidenced within the Karoo Basin; see Svensen et al., 2016) approximately 60% of the intrusions within the Ceduna sub-basin would not be imaged due to their thickness being below that which can be detected. Secondly, the thicker intrusions attenuate seismic energy, leading to a downwards decrease in the frequency of the seismic data, preventing us from detecting thinner intrusions beneath them. For instance, the frequency beneath the intrusion in Figure 3 decreases from 30 to 25 Hz immediately beneath the Base Intrusion horizon, and continues to decrease with depth. This

means it is likely that there are at least some intrusions beneath those imaged in the Nerites 3D dataset that are not successfully imaged due to the presence of overlying intrusions. Thirdly, our estimate of the volume of the intrusive complex does not account for dykes. These dykes are difficult to image in seismic data due to their steeply inclined orientation and typically narrow width (<5 m). However, the dykes played a crucial role in vertical magma transport (Reynolds et al., 2017b). For these reasons, we infer that the volume of intrusions we have provided is an underestimate.

We also note that the Nerites survey does not cover the entirety of the BBIC. Other volcanic features are found within the Bight Basin and are covered by the Flinders 2D survey. The intrusions outside the area covered by the Nerites survey mapped by Schofield and Totterdell (2008) have areas varying from 11−300 km^2 and cover a combined area of 1646 km^2. The extrusive features have areas of between 3−215 km^2 and cover a combined area of 1216 km^2. Whilst there is uncertainty in the volumes of these features, the intrusions have a larger area than the extrusive features, similar to the features observed in the Nerites survey. This suggests that the rest of the BBIC is characterised by a similar I:E ratio to that documented within our study.

How much of the erupted products have been eroded?

We infer that the volcanoes and lava flows are preserved in a near-pristine state and have not been subject to intense erosion that would significantly alter the calculated volumes of the erupted products. All volcanoes except one retain a conical shape, typical of pyroclastic cones which form in shallow marine environments (e.g. Solgevik et al., 2007). We note that only the most inboard cone displays a flat top, such as those typical of pyroclastic cones which have been eroded by wave action (e.g. Sorrentino et al., 2011). To the best of our knowledge, the lava flows are also preserved in a near-pristine state

(Reynolds et al., 2017d). The flows provide clear evidence for the direction of their emplacement and display no features suggesting they have been significantly eroded (Reynolds et al., 2017d). Furthermore, the lava flows are not offset by faults, suggesting that they have not been exposed and eroded on fault planes. Previous workers have also suggested that the vents in the Bight Basin are preserved in a condition representative of their post-eruption morphology (Jackson, 2012). Factors favouring their preservation are thought to include: 1) the volcanoes are almost exclusively located on the outer shelf and were not subjected to wave- or tide-driven erosion; 2) the post-Eocene currents were too weak to eroded the volcanoes; and 3) the volcanoes were not modified by caldera collapse (Jackson, 2012). Although we negate the importance of caldera collapse in a monogenetic field, our observations support the hypotheses of minimal erosion and we neglect the volume of eroded material in our calculations of the I:E ratio. However, our estimates likely represent a minimum value.

Magmatism along the southern Australian margin and the importance of magma host rock lithology

The eruption rate we estimate for the BBIC (~36 km^3/Myr) is intermediate between those proposed for tectonically controlled volcanic provinces (<1 km^3/Myr) and magmatically controlled volcanic provinces (>100 km^3/Myr; Valentine and Perry, 2007). This suggests that eruption rate alone cannot be used to diagnose whether the BBIC is more typical of a magmatically or tectonically controlled volcanic province. The relationship between dykes and faults is also thought to diagnostic of province type (Valentine and Perry, 2007). As detailed in the Discussion, many of the dykes in the BBIC are inferred to have been captured by faults, suggesting that this province is tectonically controlled. This is consistent with previous authors who have inferred magmatism along the southern

Australian margin results from tectonic processes such as mantle shear-driven convection and edge-driven convection (Demidjuk et al., 2007; Conrad et al., 2011; van den Hove et al., 2017b). Our results thus imply that eruption rates in tectonically controlled volcanic provinces can be substantially higher than <1 km^3/Myr (c.f. Valentine and Perry, 2007).

The best studied manifestation of volcanism along the southern Australian margin is the Newer Volcanics Province (NVP), although the I:E ratio for this province is unknown. The NVP is composed of an erupted volume ten times that within the Nerites survey (680 km^3) at a much higher rate (200 km^3/Myr; van den Hove et al., 2017b). Although most of the volcanoes and lava flows in the NVP are thought to be fed by dykes (van den Hove et al., 2017a), a small number of 1 km-wide intrusions have been described from 2D seismic data (Chatfield, 1992), whilst work by Holt et al. (2013) details a saucer-shaped sill up to 2 km in diameter from the western part of the province. Other seismic surveys within 5 km of volcanoes do not image any sills (Holt et al., 2013). Whilst there is evidence for magma storage at depth beneath tholeiitic lavas in parts of the province (McBride et al., 2001), these combined observations suggest that shallow intrusions similar in dimension (i.e. up to 23 km in diameter) to those found within the BBIC are absent from the NVP. The absence of any forced folds of similar magnitudes to those observed within the BBIC (up to 210 m in height; Jackson et al., 2013; Reynolds et al., 2017c) also suggests that sills and/or laccoliths do not form an important part of the magma plumbing system for the NVP. This scenario contrasts markedly with the BBIC, which is characterised by an abundance of sills and laccoliths which form the dominant volumetric component of the province.

A key difference between the BBIC and NVP is that dyke emplacement in approximately half of the NVP occurred through Paleozoic basement (Cas et al., 2016). In contrast, the entirety of the BBIC was constructed within a sedimentary basin. We suggest that the contrasting magma plumbing systems for the NVP and BBIC result from the

375 contrasting host rocks through which magma ascended (Fig. 9). In the case of the NVP,
376 dykes mostly ascended through brittle basement rocks and directly fed eruptions at the
377 surface. In the BBIC, magma ascended vertically through siliciclastic sediments via dykes,
378 before transitioning to sills and stalling in the shallowest subsurface, forming a voluminous
379 intrusive complex. We speculate that if the dykes in the BBIC had not ascended through a
380 sedimentary basin, more magma would have been erupted at the paleosurface and the BBIC
381 would have a lower I:E ratio.

382 We are able to negate the importance of local crustal thickness in controlling the
383 proportion of intrusive to extrusive volcanic rocks within the NVP and BBIC; the NVP is
384 found in a region where the crust is 33–38 km thick (Collins, 1991) whilst the BBIC is
385 situated above crust ~25 km thick (Ball et al., 2013). Since thicker crust is more likely to
386 promote magma cooling and stalling (Shaw, 1980), it would be expected that the NVP would
387 have a higher I:E ratio than the BBIC if crustal thickness was the dominant control. Since
388 both volcanic provinces formed after the initiation of seafloor spreading in a period of
389 tectonic quiescence, tectonic setting and the magnitude of principal stresses also cannot be
390 invoked to explain the difference in I:E ratios between the provinces.

391 There remains considerable uncertainty as to the role of magma composition and melt
392 generation rate in controlling the proportion of volcanic rocks within the provinces. Magma
393 composition may have been an important factor, although in the absence of a broader suite
394 of petrologic data from the BBIC, this remains to be confirmed. Additionally, although our
395 data suggests that the eruption rate for the NVP is much higher than that for the BBIC;
396 whether this reflects an increased melt generation rate in the mantle source region and its
397 impact on the I:E ratios of the provinces is unknown. Based on our results, which indicate
398 that I:E ratios can be highly variable and strongly influenced by local, province-specific

399 factors, we speculate that in many cases, eruption rate may be a poor measure of magma
400 productivity.

401 Our hypothesis, that the I:E ratios of the NVP and BBIC is in-part controlled by the
402 host rock through which magma ascends, is supported by a number of previous studies.
403 Earlier work has suggested that vertical magma ascent through layered sediments promotes
404 the formation of concordant intrusions (e.g. Rivalta et al., 2005; Galland et al., 2009; Taisne
405 and Jaupart, 2009). Factors that may have promoted magma stalling and sill and laccolith
406 formation in the BBIC include: 1) dykes encountering a rigidity or density barrier (Kavanagh
407 et al., 2006; Taisne and Jaupart, 2009); 2) mechanical contrasts in material toughness and
408 stiffness across an interface (Gudmundsson, 2011; Gudmundsson et al., 2014); 3)
409 delamination of host sediments (Gudmundsson, 2011); 4) hydrofracture arrest in layered
410 rocks (Gudmundsson and Brenner, 2001); 5) ascending dykes experiencing high compressive
411 stresses at weak horizontal interfaces (Maccaferri et al., 2011); and 6) magma encountering
412 lithologies that are commonly favoured by intrusions (e.g. shales; see Schofield et al., 2012).
413 Processes such as these would not operate in the Palaeozoic basement that underlies much
414 of the NVP. Our study therefore suggests that the lithology through which magma ascends
415 before reaching the surface plays an important role in controlling whether magma stalls in
416 the subsurface and the resultant I:E ratio.

417

418 **Conclusion**

419 This study has used 3D seismic data from a Mid Eocene intraplate volcanic province,
420 located offshore southern Australia, to demonstrate that seismic data provides an unrivalled
421 opportunity to determine the I:E ratios of ancient volcanic provinces. Comparable with
422 other continental volcanic provinces, the BBIC is dominantly composed of intrusions, the
423 volume of which outweighs the extrusive component by as much as two-fold. We infer that

424 the larger volume of magma stored relative to that erupted resulted from ascending dykes
425 transitioning to sills and laccoliths at shallow depths within a sedimentary basin. This
426 suggests that magma ascent through layered sediments may play an important role in
427 controlling the I:E ratios and volumes of magma erupted in other volcanic provinces.
428
429 **References**

430 Allard, P., 1997, Endogenous magma degassing and storage at Mount Etna: Geophysical
431 Research Letters, v. 24, no. 17, p. 2219-2222.
432 Annen, C., Blundy, J., and Sparks, R., 2006, The genesis of intermediate and silicic magmas in
433 deep crustal hot zones: Journal of Petrology, v. 47, no. 3, p. 505-539.
434 Ball, P., Eagles, G., Ebinger, C., McClay, K., and Totterdell, J., 2013, The spatial and temporal
435 evolution of strain during the separation of Australia and Antarctica: Geochemistry,
436 Geophysics, Geosystems, v. 14, no. 8, p. 2771-2799.
437 Cas, R., van Otterloo, J., Blaikie, T., and van den Hove, J., 2016, The dynamics of a very large
438 intra-plate continental basaltic volcanic province, the Newer Volcanics Province, SE
439 Australia, and implications for other provinces: Geological Society, London, Special
440 Publications, v. 446, p. SP446. 448.
441 Chatfield, K., 1992, The relationship between volcanics, associated intrusives and carbon
442 dioxide within the Otway Basin, South Australia: Adelaide University. BSc (Hons)
443 thesis, Adelaide, South Australia (unpublished).
444 Clarke, J., and Alley, N., Petrologic data on the evolution of the Great Australian Bight, *in*
445 Proceedings Proceedings of the Gondwana Eight Symposium: Rotterdam, AA
446 Balkema1993, p. 585-596.
447 Collins, C., 1991, The nature of the crust-mantle boundary under Australia from seismic
448 evidence: The Australian Lithosphere, v. 17, p. 67-80.

449 Conrad, C. P., Bianco, T. A., Smith, E. I., and Wessel, P., 2011, Patterns of intraplate
450 volcanism controlled by asthenospheric shear: Nature Geoscience, v. 4, no. 5, p.
451 317-321.
452 Crisp, J. A., 1984, Rates of magma emplacement and volcanic output: Journal of Volcanology
453 and Geothermal Research, v. 20, no. 3-4, p. 177-211.
454 Davies, D., Rawlinson, N., Iaffaldano, G., and Campbell, I., 2015, Lithospheric controls on
455 magma composition along Earth/'s longest continental hotspot track: Nature, v. 525,
456 no. 7570, p. 511-514.
457 Demidjuk, Z., Turner, S., Sandiford, M., George, R., Foden, J., and Etheridge, M., 2007, U-
458 series isotope and geodynamic constraints on mantle melting processes beneath the
459 Newer Volcanic Province in South Australia: Earth and Planetary Science Letters, v.
460 261, no. 3, p. 517-533.
461 Edwards, J., Cayley, R., and Joyce, E., 2004, Geology and geomorphology of the Lady Julia
462 Percy Island volcano, a late Miocene submarine and subaerial volcano off the coast of
463 Victoria, Australia: Proceedings of the Royal Society of Victoria, v. 116, no. 1, p. 15-
464 35.
465 Ferguson, D. J., Barnie, T. D., Pyle, D. M., Oppenheimer, C., Yirgu, G., Lewi, E., Kidane, T.,
466 Carn, S., and Hamling, I., 2010, Recent rift-related volcanism in Afar, Ethiopia: Earth
467 and Planetary Science Letters, v. 292, no. 3, p. 409-418.
468 Galland, O., Planke, S., Neumann, E.-R., and Malthe-Sørenssen, A., 2009, Experimental
469 modelling of shallow magma emplacement: application to saucer-shaped intrusions:
470 Earth and Planetary Science Letters, v. 277, no. 3, p. 373-383.
471 Greeley, R., and Schneid, B., 1991, Magma generation on Mars- Amounts, rates, and
472 comparisons with earth, moon, and Venus: Science, v. 254, no. 5034, p. 996-998.

473 Gudmundsson, A., 2011, Deflection of dykes into sills at discontinuities and magma-chamber
474 formation: Tectonophysics, v. 500, no. 1, p. 50-64.
475 Gudmundsson, A., and Brenner, S. L., 2001, How hydrofractures become arrested: Terra
476 Nova, v. 13, no. 6, p. 456-462.
477 Gudmundsson, A., Lecoeur, N., Mohajeri, N., and Thordarson, T., 2014, Dike emplacement
478 at Bardarbunga, Iceland, induces unusual stress changes, caldera deformation, and
479 earthquakes: Bulletin of Volcanology, v. 76, no. 10, p. 1.
480 Haederle, M., and Atherton, M. P., 2002, Shape and intrusion style of the Coastal Batholith,
481 Peru: Tectonophysics, v. 345, no. 1, p. 17-28.
482 Hansen, D. M., and Cartwright, J., 2006, The three-dimensional geometry and growth of
483 forced folds above saucer-shaped igneous sills: Journal of Structural Geology, v. 28,
484 no. 8, p. 1520-1535.
485 Holt, S., Holford, S., and Foden, J., 2013, New insights into the magmatic plumbing system of
486 the South Australian Quaternary Basalt province from 3D seismic and geochemical
487 data: Australian Journal of Earth Sciences, v. 60, no. 8, p. 797-817.
488 Iyer, H., 1984, Geophysical evidence for the locations, shapes and sizes, and internal
489 structures of magma chambers beneath regions of Quaternary volcanism:
490 Philosophical Transactions of the Royal Society of London A: Mathematical, Physical
491 and Engineering Sciences, v. 310, no. 1514, p. 473-510.
492 Jackson, C. A.-L., 2012, Seismic reflection imaging and controls on the preservation of
493 ancient sill-fed magmatic vents: Journal of the Geological Society, v. 169, no. 5, p.
494 503-506.
495 Jackson, C. A., Schofield, N., and Golenkov, B., 2013, Geometry and controls on the
496 development of igneous sill–related forced folds: A 2-D seismic reflection case study

497 from offshore southern Australia: Geological Society of America Bulletin, v. 125, no.
498 11-12, p. 1874-1890.
499 Jerram, D. A., 2002, Volcanology and facies architecture of flood basalts: Geological Society
500 of America Special Papers, v. 362, p. 119-132.
501 Johnson, R. W., Knutson, J., and Taylor, S. R., 1989, Intraplate volcanism: in eastern Australia
502 and New Zealand, Cambridge University Press.
503 Jones, J., 1969, Pillow lavas as depth indicators: American Journal of Science, v. 267, no. 2, p.
504 181-195.
505 Kavanagh, J. L., Menand, T., and Sparks, R. S. J., 2006, An experimental investigation of sill
506 formation and propagation in layered elastic media: Earth and Planetary Science
507 Letters, v. 245, no. 3, p. 799-813.
508 Keating, G., Valentine, G., Krier, D., and Perry, F., 2008, Shallow plumbing systems for small-
509 volume basaltic volcanoes: Bulletin of Volcanology, v. 70, no. 5, p. 563-582.
510 Langhi, L., Strand, J., and Ross, A. S., 2016, Fault-related biogenic mounds in the Ceduna Sub-
511 basin, Australia. Implications for hydrocarbon migration: Marine and Petroleum
512 Geology, v. 74, p. 47-58.
513 Li, Q., James, N., and McGowran, B., 2003, Middle and Late Eocene Great Australian Bight
514 lithobiostratigraphy and stepwise evolution of the southern Australian continental
515 margin: Australian Journal of Earth Sciences, v. 50, no. 1, p. 113-128.
516 Lister, J. R., and Kerr, R. C., 1991, Fluid-mechanical models of crack propagation and their
517 application to magma transport in dykes: Journal of Geophysical Research: Solid
518 Earth, v. 96, no. B6, p. 10049-10077.
519 Lu, Z., Dzurisin, D., Biggs, J., Wicks, C., and McNutt, S., 2010, Ground surface deformation
520 patterns, magma supply, and magma storage at Okmok volcano, Alaska, from InSAR

analysis: 1. Intereruption deformation, 1997–2008: Journal of Geophysical Research: Solid Earth, v. 115, no. B5.

Maccaferri, F., Bonafede, M., and Rivalta, E., 2011, A quantitative study of the mechanisms governing dike propagation, dike arrest and sill formation: Journal of Volcanology and Geothermal Research, v. 208, no. 1, p. 39-50.

Magee, C., Hunt-Stewart, E., and Jackson, C. A.-L., 2013, Volcano growth mechanisms and the role of sub-volcanic intrusions: insights from 2D seismic reflection data: Earth and Planetary Science Letters, v. 373, p. 41-53.

McBride, J.S., Lambert, D.D., Nicholls, I.A. and Price, R.C., 2001, Osmium isotopic evidnece for crust-mantle interaction in the genesis of continental flood basalts from the Newer Volcanics Province, southeastern Australia: Journal of Petrology, v. 42, p. 1197-1218.

Meeuws, F., Holford, S., Foden, J., and Schofield, N., 2016, Distribution, chronology and causes of Cretaceous–Cenozoic magmatism along the magma-poor rifted southern Australian margin: Links between mantle melting and basin formation: Marine and Petroleum Geology, v. 73, p. 271-298.

Nelson, C. E., Jerram, D. A., and Hobbs, R. W., 2009, Flood basalt facies from borehole data: implications for prospectivity and volcanology in volcanic rifted margins: Petroleum Geoscience, v. 15, no. 4, p. 313-324.

Norvick, M., 2005, Plate tectonic reconstruction of Australia's southern margins. Geoscience Australia Record, 7.

Patanè, D., Barberi, G., De Gori, P., Cocina, O., Zuccarello, L., Garcia-Yeguas, A., Castellano, M., D'Alessandro, A., and Sgroi, T., 2017, The shallow magma chamber of Stromboli volcano (Italy): Geophysical Research Letters, 44, 6589–6596, doi:10.1002/2017GL073008

546 Pinel, V., and Jaupart, C., 2004, Magma storage and horizontal dyke injection beneath a
547 volcanic edifice: Earth and Planetary Science Letters, v. 221, no. 1, p. 245-262.
548 Planke, S., Rasmussen, T., Rey, S., and Myklebust, R., Seismic characteristics and distribution
549 of volcanic intrusions and hydrothermal vent complexes in the Vøring and Møre
550 basins, *in* Proceedings Geological Society, London, Petroleum Geology Conference
551 series2005, Volume 6, Geological Society of London, p. 833-844.
552 Reynolds, P., Schofield, N., Brown, R., and Holford, S., 2017a, The architecture of submarine
553 monogenetic volcanoes–insights from 3D seismic data: Basin Research.
554 doi:10.1111/bre.12230
555 Reynolds, P., Planke, S., Millett, J., Jerram, D., Trulsvik, M., Schofield, N., and Myklebust, R.,
556 2017b, Hydrothermal vent complexes offshore Northeast Greenland: A potential
557 role in driving the PETM: Earth and Planetary Science Letters, v. 467, p. 72-78.
558 Reynolds, P., Holford, S., Schofield, N., and Ross, A., 2017c, The shallow depth emplacement
559 of mafic intrusions on a magma-poor rifted margin: an example from the Bight Basin,
560 southern Australia: Marine and Petroleum Geology,
561 doi.org/10.1016/j.marpetgeo.2017.09.008
562 Reynolds, P., Holford, S., Schofield, N., and Ross, A., 2017d, 3D seismic imaging of ancient
563 submarine lava flow fields: an example from the southern Australian margin,
564 Geochemistry, Geophysics, Geosystems.
565 Richardson, J., Connor, C., Wetmore, P., Connor, L., and Gallant, E., 2015, Role of sills in
566 the development of volcanic fields: Insights from lidar mapping surveys of the San
567 Rafael Swell, Utah: Geology, v. 43, no. 11, p. 1023-1026.
568 Rivalta, E., Böttinger, M., and Dahm, T., 2005, Buoyancy-driven fracture ascent: Experiments
569 in layered gelatine: Journal of Volcanology and Geothermal Research, v. 144, no. 1, p.
570 273-285.

571 Ryan, P., 1987, Neutral buoyancy and the mechanical evolution of magmatic systems:
572 Magmatic processes: physicochemical principles., v. 1, p. 259-287.
573 Schmincke, H.-U., 2004, Volcanism, Springer Science & Business Media.
574 Schofield, A., and Totterdell, J., 2008, Distribution, timing and origin of magmatism in the
575 Bight and Eucla Basins, Geoscience Australia.
576 Schofield, N., Holford, S., Millett, J., Brown, D., Jolley, D., R. Passey, S., Muirhead, D., Grove,
577 C., Magee, C., Murray, J., Hole, M., A.-L. Jackson, C., and Stevenson, C., 2015,
578 Regional magma plumbing and emplacement mechanisms of the Faroe-Shetland Sill
579 Complex: implications for magma transport and petroleum systems within
580 sedimentary basins: Basin Research, p. n/a-n/a.
581 Schofield, N. J., Brown, D. J., Magee, C., and Stevenson, C. T., 2012, Sill morphology and
582 comparison of brittle and non-brittle emplacement mechanisms: Journal of the
583 Geological Society, v. 169, no. 2, p. 127-141.
584 Shaw, H. R., 1980, The fracture mechanisms of magma transport from the mantle to the
585 surface: Physics of magmatic processes, v. 64, p. 201-264.
586 Skogly, O., 1998, Seismic characterization and emplacement of intrusives in the Vøring Basin:
587 Cand Scient thesis, Department of Geology, University of Oslo.
588 Smallwood, J. R., and Maresh, J., 2002, The properties, morphology and distribution of
589 igneous sills: modelling, borehole data and 3D seismic from the Faroe-Shetland area:
590 Geological Society, London, Special Publications, v. 197, no. 1, p. 271-306.
591 Solgevik, H., Mattsson, H. B., and Hermelin, O., 2007, Growth of an emergent tuff cone:
592 fragmentation and depositional processes recorded in the Capelas tuff cone, São
593 Miguel, Azores: Journal of Volcanology and Geothermal Research, v. 159, no. 1, p.
594 246-266.

595 Sorrentino, L., Cas, R. A. F., and Stilwell, J. D., 2011, Evolution and facies architecture of
596 Paleogene Surtseyan volcanoes on Chatham Islands, New Zealand, Southwest Pacific
597 Ocean: Journal of Volcanology and Geothermal Research, v. 202, no. 1, p. 1-21.
598 Svensen, H. H., Polteau, S., Cawthorn, G., and Planke, S., 2016, Sub-volcanic Intrusions in the
599 Karoo Basin, South Africa: Berlin, Heidelberg, Springer Berlin Heidelberg, p. 1-14.
600 Taisne, B., and Jaupart, C., 2009, Dike propagation through layered rocks: Journal of
601 Geophysical Research: Solid Earth, v. 114, no. B9, p. n/a-n/a.
602 Taisne, B., and Tait, S., 2011, Effect of solidification on a propagating dike: Journal of
603 Geophysical Research: Solid Earth, v. 116, no. B1.
604 Thomson, K., 2005, Volcanic features of the North Rockall Trough: application of
605 visualisation techniques on 3D seismic reflection data: Bulletin of Volcanology, v. 67,
606 no. 2, p. 116-128.
607 Valentine, G. A., and Perry, F. V., 2007, Tectonically controlled, time-predictable basaltic
608 volcanism from a lithospheric mantle source (central Basin and Range Province,
609 USA): Earth and Planetary Science Letters, v. 261, no. 1–2, p. 201-216.
610 van den Hove, J., Grose, L., Betts, P. G., Ailleres, L., Van Otterloo, J., and Cas, R. A. F.,
611 2017a, Spatial analysis of an intra-plate basaltic volcanic field in a compressional
612 tectonic setting: South-eastern Australia: Journal of Volcanology and Geothermal
613 Research, v. 335, p. 35-53.
614 van den Hove, J. C., Van Otterloo, J., Betts, P. G., Ailleres, L., and Cas, R. A., 2017b,
615 Controls on volcanism at intraplate basaltic volcanic fields: Earth and Planetary
616 Science Letters, v. 459, p. 36-47.
617 Vidal, V., and Bonneville, A., 2004, Variations of the Hawaiian hot spot activity revealed by
618 variations in the magma production rate: Journal of Geophysical Research: Solid
619 Earth, v. 109, no. B3.

620 Wadge, G., 1980, Output rate of magma from active central volcanoes: Nature, v. 288, no.
621 5788, p. 253-255.
622 Wellman, P., and McDougall, I., 1974, Cainozoic igneous activity in eastern Australia:
623 Tectonophysics, v. 23, no. 1-2, p. 49-65.
624 White, S. M., Crisp, J. A., and Spera, F. J., 2006, Long-term volumetric eruption rates and
625 magma budgets: Geochemistry, Geophysics, Geosystems, v. 7, no. 3.

626

627 **Figure captions**

628 **Fig. 1.** Geological map and stratigraphic column (A) for the Bight Basin Igneous Complex
629 (BBIC) and seismic line from the Flinders 2D survey showing the volcanic features (B).
630 **Fig. 2.** Map showing the location of the Bight Basin Igneous Complex (BBIC), the Newer
631 Volcanics Province (NVP), the Older Volcanics Province (OVP) and the Macedon-Trentham
632 Province (MTP) along the southern Australian margin. Adapted from Meeuws et al. (2016).
633 **Fig. 3.** Seismic cross sections of vent with a lava flow at its base (A) and an intrusion (B).
634 See Fig. 5 for their location.
635 **Fig. 4.** Figure demonstrating the method used to calculate the volume of the intrusions.
636 Part A shows a schematic illustration of the horizons picked and the velocities used. Where
637 the intrusion is represented by a single trough-peak doublet, its thickness is below the
638 resolution of the seismic data and above the detection limit (i.e. between 4 and 45 m thick).
639 An example of an intrusion and the picked horizons are shown in part B. Part C shows how
640 the total area of the intrusion (between points 1 and 4) can be sub-divided into areas >45 m
641 thick (within the dashed line) and areas below the resolution limit (between the dashed line
642 and the outline of the intrusion). Notice that points 1, 2, 3 and 4 on the plan view correlate
643 with the picks on part A and B of the figure. Part D shows amplitude (left) and thickness
644 maps (right) for the intrusion in part B. Note that the true thickness of the intrusion

beneath 45 m is unknown. The values used to calculate the maximum and minimum volume of the intrusion are shown beneath. See Fig. 5 for the location of the intrusion.

Fig. 5. Map showing the distribution of igneous features in the Nerites survey.

Fig. 6. Charts showing the volume of the individual components of the BBIC and the sum of its components.

Fig. 7. Graph comparing the volume of the intrusive and extrusive components of continental (blue) and oceanic (orange) volcanic provinces. Data from this study is shown as a green point with an error bar representing the potential range in volume of the intrusions. Data from White et al. (2006) and references there-in.

Fig. 8. Graph showing the relationship between the volumes and duration of volcanism. The volcanic fields are classified accoring to their SiO_2 content, as determined by White et al., (2006). The BBIC plots at the lowest end of the field for basaltic fields whilst the NVP has a volume more typical of the mean value of basaltic volcanic fields. Adapted from White et al. (2006); data for the NVP taken from Cas et al. (2016).

Fig. 9. Schematic diagram illustrating the contrasting plumbing systems and I:E ratios for the Newer Volcanics Province (NVP) and the Bight Basin Igneous Complex (BBIC). In the case of the northern part of the NVP, volcanoes are fed by dykes that ascend through basement directly to the surface. In the BBIC, dykes ascend through basement and into the sediments of the Ceduna sub-basin. Factors such as rigidity or density barriers; mechanical contrasts in material stiffness across bedding planes; delamination of host sediments; hydrofracture arrest and dykes experiencing high compressive stresses at bedding planes may have triggered the dykes to transition into sills (see text for references). This resulted in greater volumes of magma being stored in the subsurface relative to the NVP. Adapted from van den Hove et al. (2017a).

Table 1. *Summary measurements of volcanic features observed in the Nerites survey. * DRE*

Acknowledgements

This work comprises a part of the Great Australian Bight Deepwater Marine Program (GABDMP). The GABDMP is a CSIRO research program, sponsored by Chevron Australia the results of which will be made publicly available. 3D seismic data was gratefully provided by TGS. We thank IHS for access to Kingdom seismic interpretation software and DownUnder GeoSolutions for access to DUG Insight. The constructive reviews provided by Sebastian Watt and Jozua van Otterloo are gratefully acknowledged.

Table

Feature	Min. vol. (km^3)	Max. vol. (km^3)	Min. Height/thickness (m)	Max. Height/thickness (m)	Min. Length/diameter (km)	Max. Length/diameter (km)	Area covered (km^2)	Combined volume (km^3)	DRE (km^3)	Total lava/magma volume within Nerites survey
Vents	0.1	11	60	625	0.5	10	602	70	58	158–187*
Lava flows	0.01	9	5	45	0.4	34	558	20	8–18	
Intrusions	0.1	13	5	270	2	23	1537	92–111	NA	

Table 1.

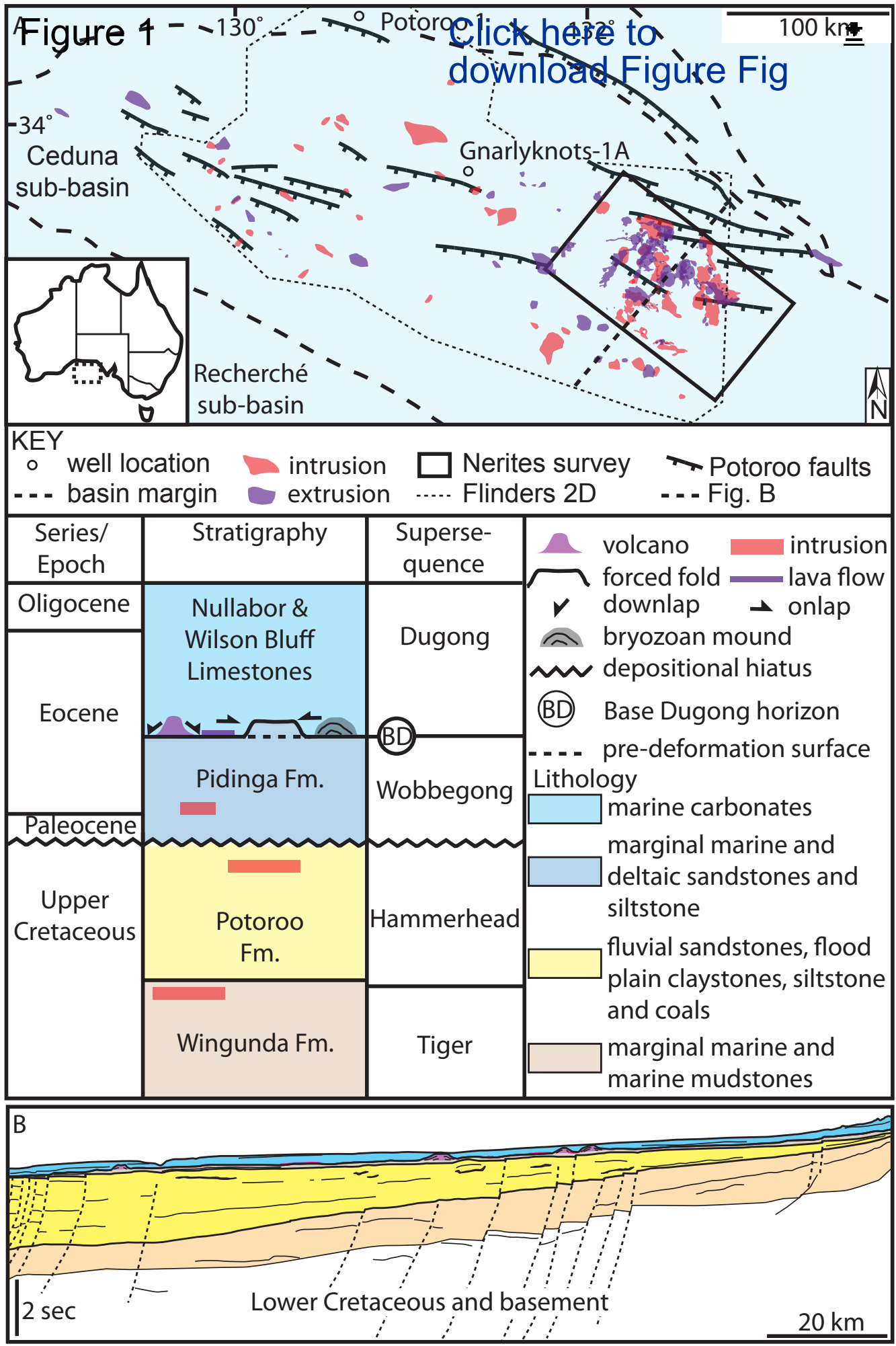
Figure 1
Click here to download Figure Fig
A
130°
Potoroo-1
132°
100 km
34°
Ceduna sub-basin
Gnarlyknots-1A
Recherché sub-basin
N
KEY
well location
basin margin
intrusion
extrusion
Nerites survey
Flinders 2D
Potoroo faults
Fig. B
Series/ Epoch
Stratigraphy
Superse-quence
Oligocene
Eocene
Paleocene
Upper Cretaceous
Nullabor & Wilson Bluff Limestones
Pidinga Fm.
Potoroo Fm.
Wingunda Fm.
Dugong
BD
Wobbegong
Hammerhead
Tiger
volcano
intrusion
forced fold
lava flow
downlap
onlap
bryozoan mound
depositional hiatus
Base Dugong horizon
pre-deformation surface
Lithology
marine carbonates
marginal marine and deltaic sandstones and siltstone
fluvial sandstones, flood plain claystones, siltstone and coals
marginal marine and marine mudstones
B
2 sec
Lower Cretaceous and basement
20 km

Figure 2

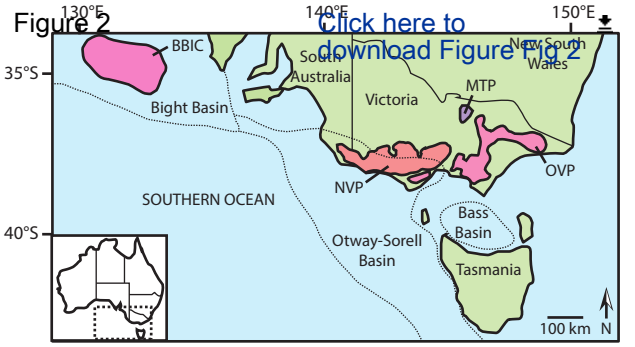

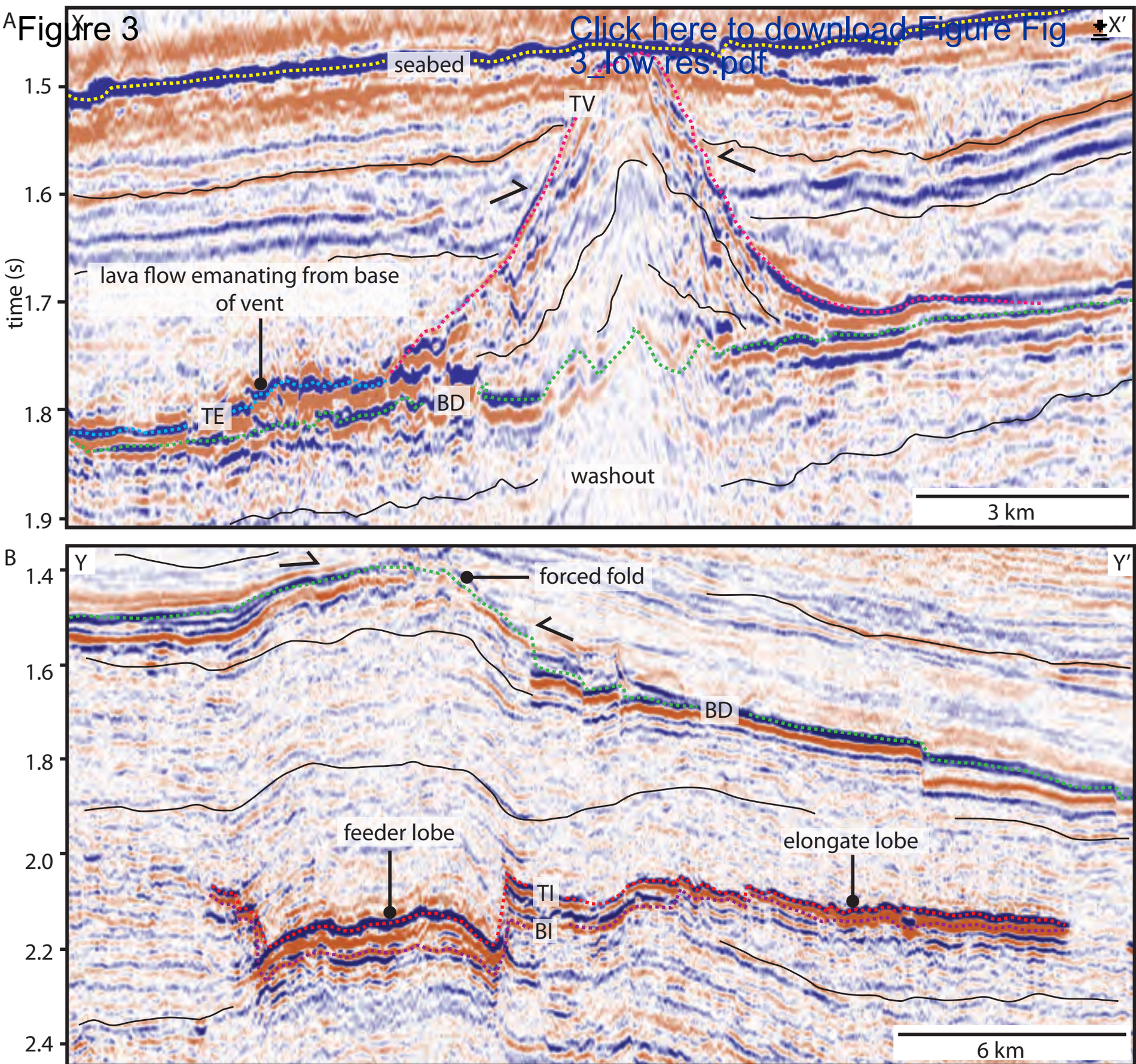

Figure 3

Click here to download Figure Fig 3_low res.pdf

TGS

Figure 4

Click here to download Figure Fig

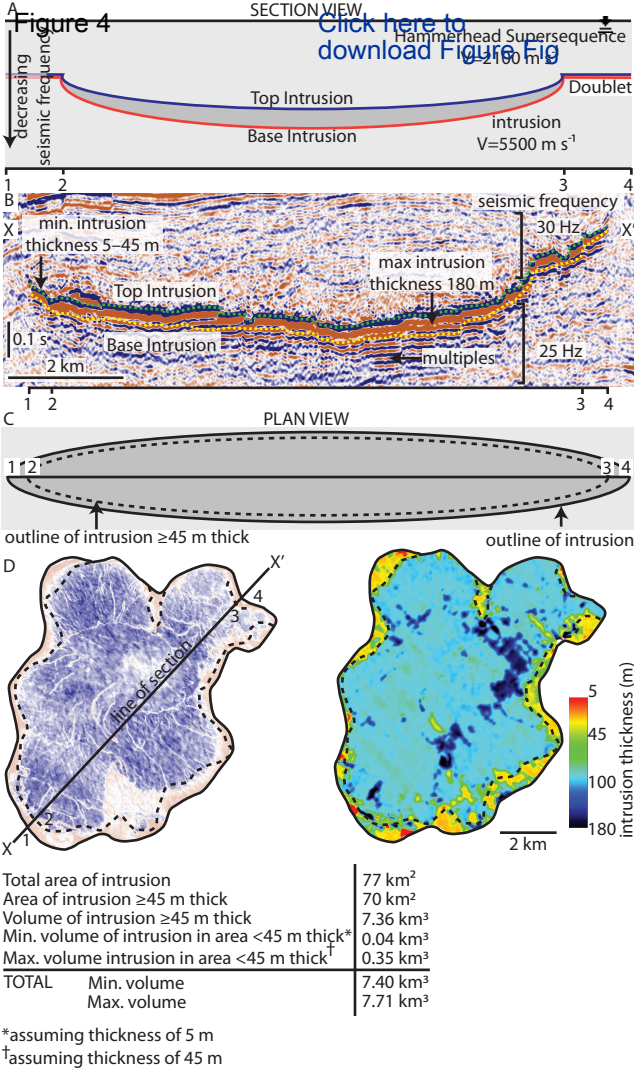

Total area of intrusion		77 km²
Area of intrusion ≥45 m thick		70 km²
Volume of intrusion ≥45 m thick		7.36 km³
Min. volume of intrusion in area <45 m thick*		0.04 km³
Max. volume intrusion in area <45 m thick†		0.35 km³
TOTAL	Min. volume	7.40 km³
	Max. volume	7.71 km³

*assuming thickness of 5 m

†assuming thickness of 45 m

Figure 5

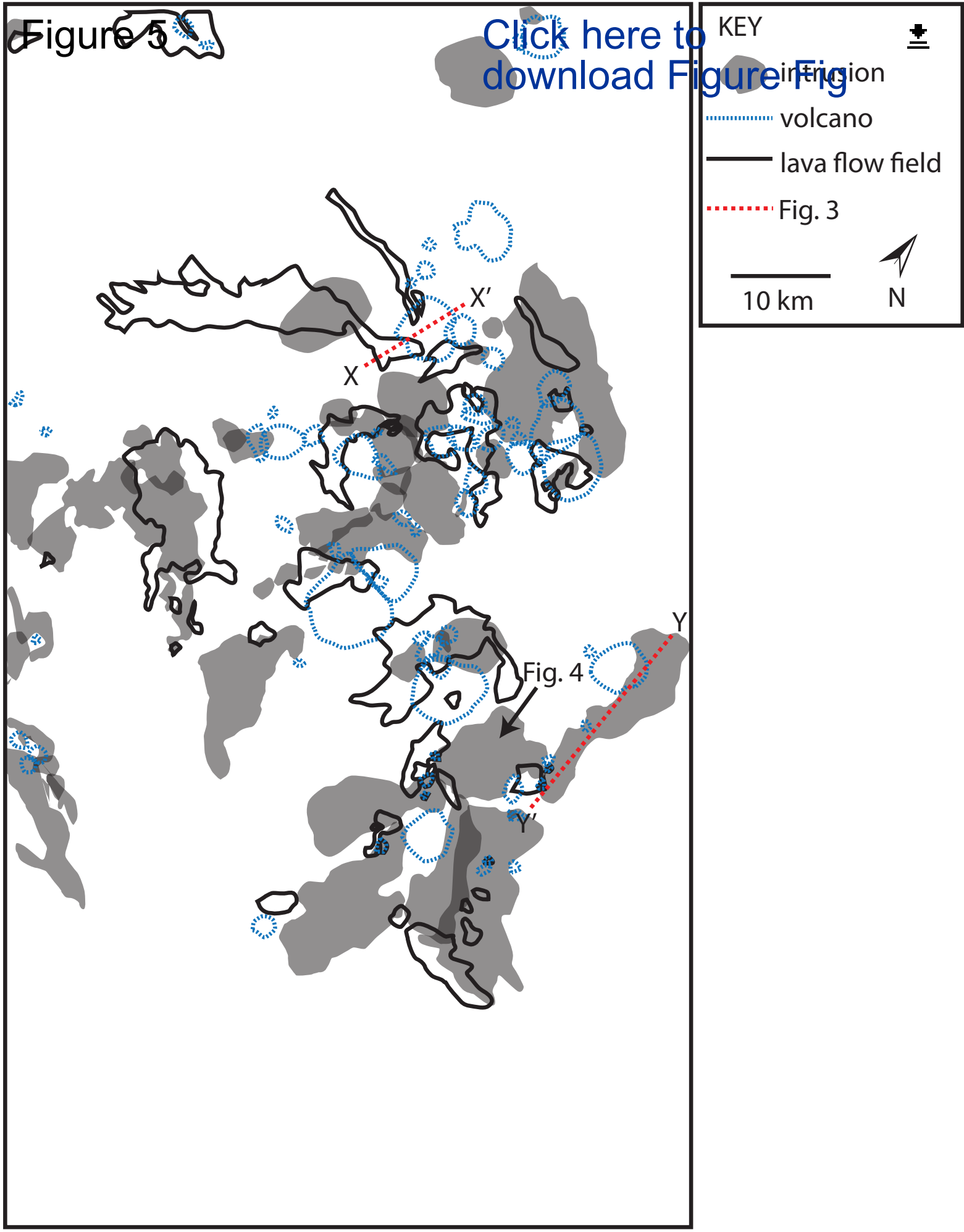

Figure 6

Click here to download Figure Fig

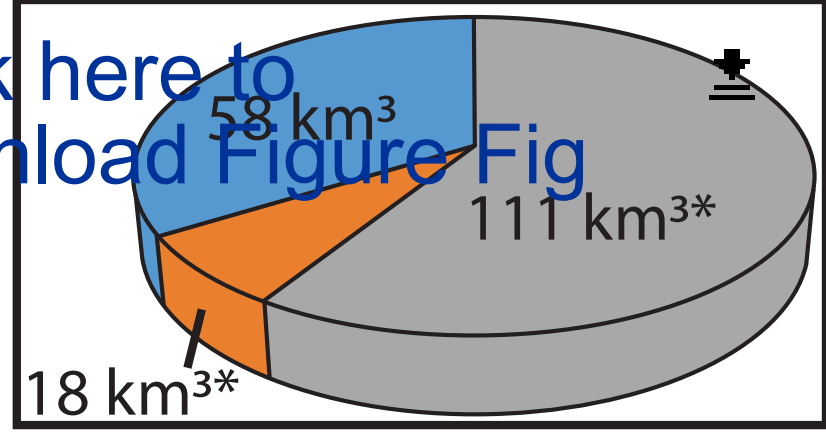

Figure 7

Click here to download Figure Fig

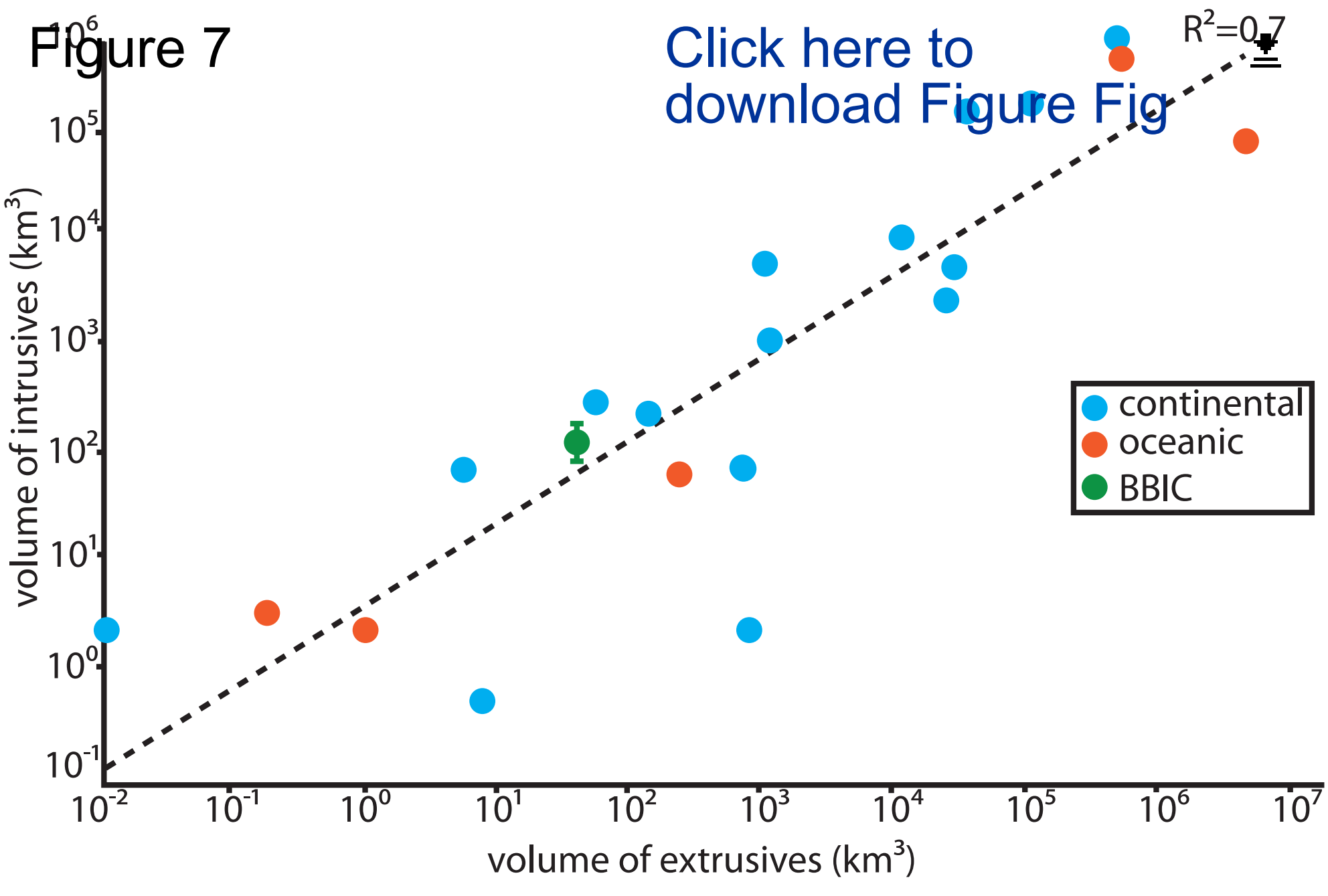

Figure 8

Click here to download Figure figure 8 revised.pdf

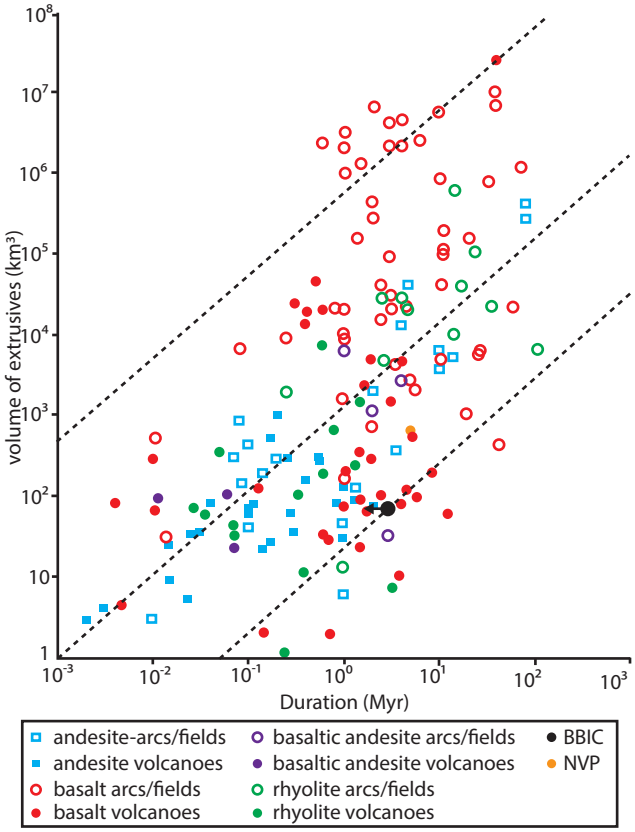

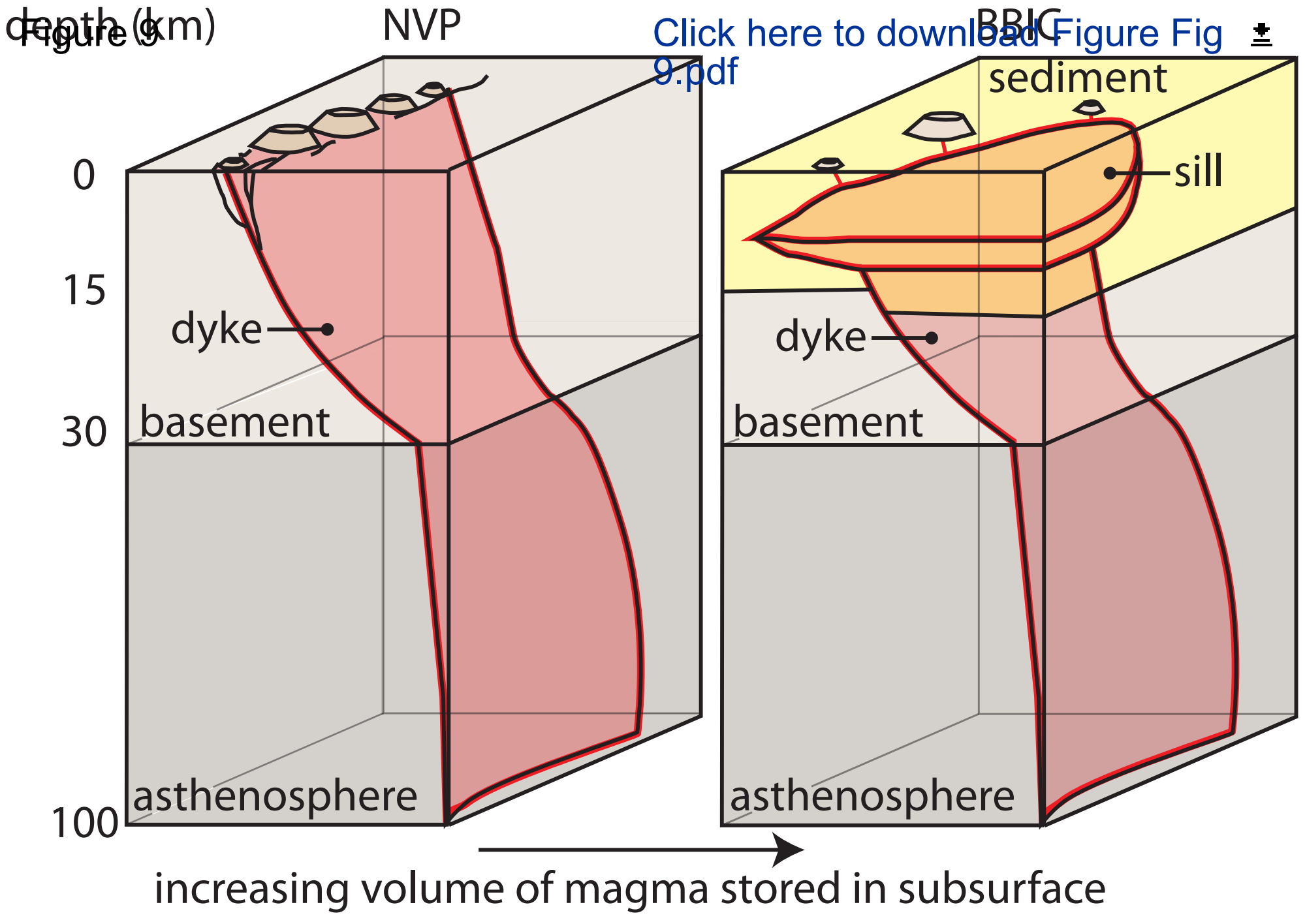

morphology of which is linked to their emplacement depth, host sediment rheology and the physical properties of the magma. This plumbing system contrasts markedly with those found along better-studied volcanic rifted margins.